International Journal of Mass Spectrometry 308 (2011) 239–252

Contents lists available at ScienceDirect

International Journal of Mass Spectrometry

journal homepage: www.elsevier.com/locate/ijms

Spectroscopically resolved competition between dissociation and detachment from nitrobenzene radical anion

Jeffrey D. Steill [a,*], Jos Oomens [a,b]

[a] FOM Institute for Plasma Physics Rijnhuizen, Edisonbaan 14, 3439MN Nieuwegein, The Netherlands
[b] van't Hoff Institute for Molecular Sciences, University of Amsterdam, Science Park 904, 1098XH Amsterdam, The Netherlands

ARTICLE INFO

Article history:
Available online 10 August 2011

Dedicated to Prof. John R. Eyler on the occasion of his 65th birthday, honoring his contributions in IRMPD ion spectroscopy and mass spectrometry in general.

Keywords:
Nitrobenzene
Radical anion
IRMPD
Electron detachment
QET
Distonic ion

ABSTRACT

We report the vibrational spectrum of the gas-phase isolated nitrobenzene radical anion. The spectrum has been acquired by infrared multiple-photon absorption induced dissociation and electron detachment using the FT mass spectrometer coupled to the infrared free-electron laser FELIX. Upon wavelength-dependent multiple-photon absorption of intense IR irradiation, the vibrational spectrum acquired by on-resonance dissociation to NO_2^- was shown to correlate with the more sensitive electron detachment channel which is indirectly observed by using SF_6 as electron scavenger. The spectrum is compared to previous spectroscopic studies and novel DFT calculations. The frequency and intensity changes of the vibrational bands for the radical anion with respect to the neutral are interpreted with the aid of molecular orbital calculations and mode projection analysis. The vibrations of the neutral and the anion are interpreted in terms of the component benzene modes. The anion shows a reversal of the familiar strongly deactivating meta-directing electrophilic aromatic substitution effect of the neutral due to a resonance effect placing electron density at the ortho- and para-positions, resulting in a structure of distonic character. The greater abundance of the electron detachment channel over the NO_2^- loss dissociation channel is interpreted in terms of statistical models of the energy-dependent unimolecular rates. The anion and neutral vibrational frequencies employed in a quasi-equilibrium theory (QET) model of electron detachment compare favorably to previous experimental results of metastable anion autodetachment lifetimes. The ratio of dissociation to detachment is investigated as a function of FEL power and the competition between these channels is in agreement with a statistical model.

Published by Elsevier B.V.

1. Introduction

Both the electron attachment and dissociation properties of nitroaromatic compounds are ultimately responsible for their utility as explosives. One of the initial reaction steps involves electron transfer and the NO_2 loss is the key step. Nitroaromatic compounds are also essential components of chemical synthesis; the simplest example, nitrobenzene, is of unique importance as the primary source for industrial aniline synthesis via a hydrogenation reaction. The nitro group serves as a classic case of a deactivating, meta-directing electrophilic aromatic substitution agent, due to the unimportance of π-resonances donating electron density to the ring in favor of resonances placing electron density on the nitro-substituent. The relative unimportance of the π-resonance between the nitrogen and aromatic ring results in the dominance of inductive effects removing electron density from the ring. The strength of this effect is sufficient to inspire curiosity regarding the influence of electron attachment upon this property.

The electron withdrawing effect of the nitro-moiety is related to the large electron affinity of the neutral and hence overall stability of the radical anion. The electron affinity (EA) of NO_2 is 2.2 eV [1] while that of nitrobenzene is 1.0 eV [2]. However, the stabilization of the excess charge in the anion is also facilitated in large part by the phenyl system. The EA of the phenyl C_6H_5 radical is 1.1 eV [3], as compared to the only barely positive EA of the methyl radical (CH_3) [4]. This results in a large difference between the electron affinities of nitrobenzene and nitromethane (EA = 0.2 eV) [5,6], demonstrating the importance of the aromatic resonance in the nitrobenzene anion. The apparent importance of the phenyl system in stabilizing the excess charge of the nitrobenzene anion again leads to the question of the charge distribution in the anion and the change in bonding properties relative to the neutral. A particularly sensitive probe of these properties is vibrational spectroscopy, as shifts in vibrational band positions and intensities reveal changes in the bonding properties between neutral and charged species, particularly when complemented with computational analysis. The current study addresses the bonding properties of the anion with

* Corresponding author at: Sandia National Laboratories, Combustion Research Facility, 7011 East Avenue, Livermore, CA 94551-0969, USA. Tel.: +1 925 294 4511.
E-mail addresses: jdsteil@sandia.gov, jsteill@gmail.com (J.D. Steill).

1387-3806/$ – see front matter. Published by Elsevier B.V.
doi:10.1016/j.ijms.2011.08.001

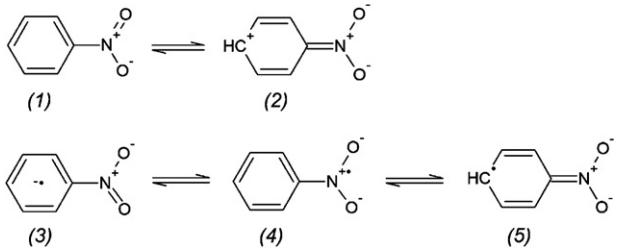

Scheme 1.

the methodology of mass spectrometry based vibrational action spectroscopy in Penning traps as pioneered by the groups of Eyler, Beauchamp, Brauman and others [7].

The bonding properties of the radical anion have been investigated in the condensed phase by electron spin resonance (ESR) of nitrobenzene reduced in solution [8]. These studies suggested an interesting relationship between the neutral and the anion in terms of the resonance interaction of the nitro group with the ring. As shown in Scheme 1, the familiar primary structure of relevance for the nitrobenzene neutral is the pair of structures represented here with a single structure labeled (1) that places partial negative charge on the oxygen atoms to result in partial NO double-bond character and only σ-character for the CN bond. The possible resonance involving π-bond character of the CN bond labeled as (2) results in a large partial positive charge on the ring and single-bond character of the NO bonds, which is at best not strongly favored [9]. As shown by structure (3), a similar partial double NO bonding structure, as favored for the neutral, can be drawn for the radical anion where the excess charge is delocalized around the ring. Although this resonance structure may not be unimportant, the other structures shown as (4) and (5) are likely more relevant. The distonic radical ion structure shown as (5) is in fact best represented as two resonance structures itself, the one shown, and one placing the radical in the ortho-position. This situation is reminiscent of an aromatic electrophilic activation agent, and in fact the ESR studies [8] demonstrated exactly this property; the anion shows significantly more spin density at the para- and ortho-positions than at the meta-position, suggesting a reversal of the strength of the resonance interaction of the nitro group with the aromatic ring. These ESR studies showed that there is a sharing of the radical character between the nitrogen (resonance structure 4) and the ortho- and para-carbons (resonance structure 5), which explains the calculated shortening of the CN bond in the anion [10]. There are numerous other observable properties that can be expected to manifest this change: vibrational band shifts and torsional barriers, in particular. In addition, computed properties such as charge densities and molecular orbitals [10] can shed further insight on the bonding characteristics of the anion.

In addition to the numerous studies of the nitrobenzene radical anion in the condensed phase, the interesting gas-phase electron attachment behavior of nitrobenzene anion is also well characterized. The nitrobenzene molecule is known to attach low-energy electrons into both dipole-bound [2,11] and valence-bound states [2,12], as well as showing multiple resonances from anionic excited states [2,13,14]. Nitrobenzene has a relatively large cross-section for associative free-electron attachment at zero electron energy [12,14] and the metastable parent anion formed shows a significant lifetime towards autodetachment (on the order of tens of μs to ms) [11,12,15]. Both associative and dissociative electron attachment are known to occur, and many examples of the dissociation of nitrobenzene to produce the NO_2^- ion have been observed from relatively low-energy electrons [13,14,16]. While higher energy scattering resonances are implicated in dissociative electron attachment at certain energies, Pelc et al. [14] identified a low-energy dissociative resonance that corresponds to the expected dissociation energy from the electronic ground state. Thus, due to the comparable efficiencies of dissociation and detachment, the ion may be expected to show a competition between these processes upon activation.

The characteristics and stability of the anion have previously been spectroscopically investigated by photoelectron [2], vibrational autodetachment [6,17] and matrix-isolation IR [10] methods. The spectroscopy has established that the nitrobenzene anion undergoes a significant overall red-shift of most vibrational modes, induced by a significant structural change of the anion relative to the neutral [10] that can be related to the anti-bonding properties of the lowest unoccupied molecular orbital (LUMO) of the neutral and highest occupied molecular orbital (HOMO) of the anion. Particularly the N–O bonds as well as the C–N bond are of interest in this respect [10]. These studies are in agreement with the condensed-phase ESR results, namely, the weakening of the bonding in nitrobenzene upon electron attachment is not global, but rather highly localized and results in the strengthening of certain bonds at the expense of others.

The vibrational spectroscopy of negative ions in the condensed phase is common, and matrix-isolation infrared absorption spectroscopy provides a great improvement to solution-phase spectra by reducing the perturbation from the environment. The infrared spectroscopy of gas-phase anions, however, is a developing field for both complexed and isolated species. As discussed in several recent review articles [7,18,19], the vibrational spectroscopy of negative ions is greatly facilitated by infrared action spectroscopies such as vibrational predissociation, vibrational autodetachment, and infrared multiple-photon dissociation and detachment (IRMPD). The particular advantage of IRMPD spectroscopy is that it provides an opportunity for measurement free of intermolecular perturbation in the IR "fingerprint" region even in strongly bound negative ions. Although comparisons of cationic IRMPD spectra to vibrational predissociation spectra and matrix-isolation IR spectra demonstrate the matrix perturbations are typically of small consequence [20], the vibrational spectroscopy of gas-phase anions is relatively less explored, and it is thus essential to consider the effect of the environment. Most gas-phase anionic IRMPD studies to date have focused on the conjugate bases of closed-shell organic [21–28] or inorganic acids [29] (or complexes thereof [30–34]), or transition metal clusters [35,36], but fewer studies [37–39] have examined the spectroscopy of stable radical anions formed via direct electron attachment processes, a class of anions for which numerous vibrational predissociation and matrix-isolation studies have been reported. A recent comparison of matrix-isolation, vibrational predissociation, and IRMPD spectra for the SF_6^- and SF_5^- radical anions [37,40,41] demonstrated rough agreement between the methods, but few bands were available for comparison. A similar situation exists for the C_{60}^- radical anion, also with very few IR-active bands [38,42]. The current study provides an opportunity for direct comparison of a radical anion with a significant number of active vibrational bands to derive a more quantitative measure of agreement.

The use of multiple-photon absorption of negative ions stored in ion traps for action spectroscopy has been reviewed, but few have discussed the relevance of the method for negative ion dynamics [43,44]. IRMPD spectroscopy of negative ions is a multidimensional tool as it inherently contains information about the competition between electron detachment and dissociation. This is analogous to the competition between dissociation and thermionic emission observed in strongly bound neutral molecules such as C_{60} [45]. In this sense it provides a unique opportunity to relate to the previously observed phenomenon of metastable negative ions formed from free-electron attachment [12,46]. IRMPD of a negative ion can be considered as a comparative study to free-electron attachment

processes because what is ultimately observed is the decay from anions in a similarly energized state. Thus, it is reasonable to expect statistical models of thermionic emission to be equally appropriate in both cases. The success of a free-electron laser infrared light source for providing sufficient power to create conditions for observation of simultaneous electron detachment and dissociation, even in strongly bound anions, has been demonstrated [22,37]. Simultaneous detection of the yield from photodetachment and photodissociation processes constrains a statistical unimolecular dynamics model to reconcile their observed relative abundances with the relationship between internal energy and laser power.

Detection of photo-induced ionic fragmentation in an ion-trap apparatus such as a Fourier-transform ion cyclotron resonance mass spectrometer (FTICR-MS) is straightforward; definitive photodetachment detection of ejected electrons is not. The utility of 'electron scavenger' molecules in this capacity has been described previously [47,48]. Earlier studies with cw and pulsed CO_2 lasers have demonstrated that the electron scavenger method coupled with multiple-photon infrared absorption of anions trapped in FTICR-MS instruments can provide a means for study of IR-induced electron detachment. The exceptional electron-capture cross-sections and large electron affinities of these species make them useful for the detection of low-energy free electrons, especially in the case of ICR cells. The additional properties of chemical inertness and spectral transparency over large wavelength regions [37] make the method ideal for detection of electron detachment from infrared irradiated molecular anions. The previous examples of vibrational action spectroscopy of gas-phase molecular anions based on electron detachment have been recently improved upon by the use of tunable IR radiation from a FEL source [22,37,38].

The detailed examination of the competition between detachment and dissociation from a molecular anion in this spirit was performed for a very similar ion, the m-fluoronitrobenzene radical anion [49]. Models of these unimolecular reactions require even at bare minimum a variety of parameters: a threshold dissociation energy, transition-state characterization, electron affinity, electron-capture cross-sections, and vibrational frequencies of reactants and products. Thus, in addition to establishing inherent bonding properties of the anion, vibrational spectroscopy is essential for constraining the model parameters of unimolecular reaction dynamics. The current effort extends the previous treatment by providing an experimental constraint for many of these often-approximated parameters; the spectroscopic information is utilized to improve the modeling of the unimolecular dynamics underlying its acquisition. IRMPD of the nitrobenzene anion thus provides an opportunity to simultaneously investigate the bonding properties and decomposition dynamics of a fundamentally important negative ion.

2. Experimental methods

2.1. ESI and FTICR mass spectrometry; IRMPD

Nitrobenzene radical anions are generated by the use of a commercial Micromass "Z-spray" electrospray ionization (ESI) source. A solution/suspension of 1.2 mg/mL nitrobenzene in 60:40 MeOH:H_2O was made by adding 0.013 mg of the neat sample to 10 mL of the solvent and shaking directly before injection into the ESI at a flow rate of 10 μL/min. Conditions optimized to produce the radical anion were an ESI needle utilizing dry N_2 gas flow and a needle voltage of −3 kV, cone voltage of −90 V, and temperatures of 90 and 50 °C on the needle and cone assemblies, respectively. Ions were accumulated for approximately 5 s in a hexapole trap with an axial trapping well potential of 4–5 V before subsequent storage in the Penning trap of a homebuilt Fourier-Transform Ion Cyclotron Resonance Mass Spectrometer (FTICR-MS) that has been described previously [50]. Mass isolation of the nitrobenzene anion (*m/z* 123) was done by the SWIFT [51] method utilizing a modified version of the datastation and software of Heeren and co-workers [52]. After allowing 2 s for radiative and collisional cooling the ions were irradiated by IR in the range of 6–16 μm generated by FEL at our institute (FELIX) [53]. FELIX produces continuously tunable IR radiation at pulse energies of ∼50 mJ per macropulse of approximately 5 μs. The bandwidth of the FEL is less than 1% of the central wavelength over the range of 6–16 μm. The ions are irradiated for 3–4 s at a macropulse repetition rate of 5 Hz. At each spectral point three mass spectra are recorded and averaged. The IRMPD yield spectrum is produced by dividing the sum of the product ion(s) by the sum of parent and product ions as a function of FEL wavelength. The spectra are averages of multiple runs, including a spectral scan scaled by a factor of 2 recorded with the FEL at a power of 50% of previous runs. The background pressure in the cell without an electron-capture gas was 5×10^{-8} Torr. With addition of the background electron scavenger gas SF_6, the ICR cell pressure increased to approximately 6×10^{-8} Torr. The mass isolation of the nitrobenzene anion and subsequent on-resonance FEL irradiation produced the NO_2^- ion (*m/z* 46). No other dissociation channel was observed, but more on-resonance parent ion depletion was observed than was accounted for in the NO_2^- dissociation channel. Upon addition of a background pressure of approximately 10^{-8} Torr of SF_6 to the ICR cell, SF_6^- (*m/z* 146) production was observed on resonance with the depletion and dissociation channels. By comparison of spectral runs with and without scavenger present, it was determined that the dissociation and detachment spectra could be acquired simultaneously. The depletion spectrum of the parent anion and the appearance of NO_2^- was verified to be identical with and without scavenger gas present (Supplementary Information (S1)), thus obviating the question of influence of the scavenger on the parent. The SF_6^- anion was shown to be transparent to the FEL with regard to further IRMPD in the spectral region investigated [37].

2.2. Computational methods

To aid in the interpretation of experimental results and provide a basis for a theoretical discussion, electronic structure calculations are performed. Minimum energy geometries and harmonic vibrational frequencies for the nitrobenzene neutral, radical anion, and dissociative fragments were computed by hybrid-DFT methods implemented within Gaussion03 [54], using a range of basis sets from 6-311++G** to aug-cc-pVTZ. The nitrobenzene neutral molecule, phenide ($C_6H_5^-$) and NO_2^- anion were calculated as closed-shell singlet states, and the nitrobenzene anion, NO_2, NO and C_6H_5 neutral fragments were calculated as open-shell doublet states using spin-unrestricted methods. Dissociation (such as NO_2^- loss) and detachment (i.e. e^- loss) energies were investigated using both Hybrid-DFT (B3LYP) and coupled-cluster (CCSD(T)) methods. For the CCSD(T) calculations, energies are computed at the B3LYP/aug-cc-pVTZ optimized geometries. Zero-point energy corrections are applied to the thermodynamic parameters (zero Kelvin) at the level of theory used, except for CCSD(T) values, which are corrected according to the unscaled B3LYP/aug-cc-pVTZ harmonic vibrational frequencies. For comparison to experiment, computed harmonic vibrational frequencies of the nitrobenzene anion and neutral are scaled by a factor of 0.979. Optimized geometric structures of these calculations are provided in Supplementary Information (S2). Other computational investigations such as constrained optimizations, natural population analysis, and molecular orbital calculations were performed with the B3LYP functional and either the aug-cc-pVTZ or 6-311++G(2d,2p) basis sets. Finally, the B3LYP/aug-cc-PVTZ harmonic frequency calculations for benzene, nitrobenzene neutral and nitrobenzene anion were employed for

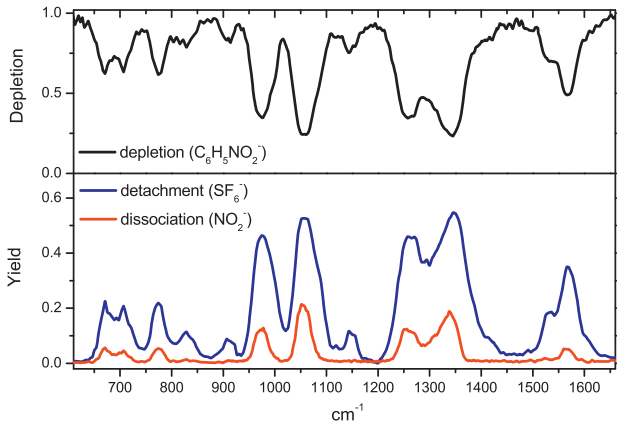

Fig. 1. Experimental IRMPD spectrum of the nitrobenzene anion obtained using the tunable IR radiation from an FEL. Shown in the upper panel is the resonant $C_6H_5NO_2^-$ parent ion depletion and in the lower panel are the correlated NO_2^- dissociation fragment yield and the SF_6^- electron scavenger yield, which serves as a proxy for the detachment yield from the irradiated negative ion.

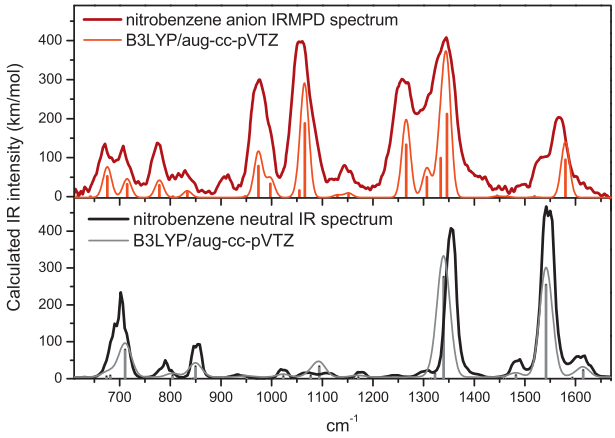

Fig. 2. Comparison of experimental and computed IR spectra for nitrobenzene neutral and anion. The upper panel displays the negative log of the anion IRMPD depletion spectrum shown in Fig. 1, and the lower panel shows a gas-phase IR absorption spectrum of nitrobenzene from the NIST Chemistry Webbook. Overlaid on each experimental spectrum is the B3LYP/aug-cc-pVTZ scaled (0.979) harmonic frequency stick spectrum and a simulated spectrum from a convolution with a Gaussian lineshape of 20 cm^{-1} width.

use with the vibrational projection analysis (ViPA) code of Grafton and Wheeler [55,56].

3. Results and discussion

3.1. Anion IRMPD spectral interpretation and comparison

While electrospray ionization is typically expected to produce closed-shell solution-stable ions, the one-electron reductive capacity of nitrobenzene [8], the large low-energy associative electron-capture cross-section [12] and the significant ion-molecule collisional electron transfer capability[57] provide ample rationale for the observation of the radical anion from the ESI process. Since the nitrobenzene anion signal was ample and stable, no attempt was made to enhance the anion production by adding a reducing agent to the electrospray solution. Upon on-resonance irradiation with the infrared laser, both SF_6^- and NO_2^- were observed, demonstrating that the laser power in this experiment is sufficient to energize the anion towards both electron detachment and dissociation processes. As shown in Fig. 1, the on-resonance production of SF_6^- via electron detachment was determined to be more facile than dissociation forming NO_2^-. The SF_6^- signal correlates best with the photo-depletion of the parent anion and reveals subtleties in the detachment action spectrum that are missing in the dissociation channel. For instance, the detachment channel reveals features that are not present or much weaker in the dissociation channel, such as resonances at 1530 cm^{-1}, 1150 cm^{-1}, 910 cm^{-1}, and 830 cm^{-1}. Overall though, other than the lack of sensitivity in the dissociation channel, there is no severe difference between the spectra as acquired by the depletion, dissociation and detachment channels. The spectrum provides an abundance of spectral detail in the wavelength region investigated which we analyze based on DFT harmonic frequency calculations. While it is interesting to consider the 'missing' features of the dissociation channel as a possible manifestation of vibrational mode-selectivity, comparison to DFT calculations show that these features correlate to weakly IR-active bands from all three of the IR-active symmetry vibrations. Thus there is no correspondence with symmetry of the vibration and the difference between the channels is likely due solely to reduced sensitivity.

Shown in the upper panel of Fig. 2 is the experimental depletion spectrum compared to the B3LYP/aug-cc-pVTZ calculated nitrobenzene frequencies scaled by 0.979 and convoluted with a 20 cm^{-1} FWHM Gaussian lineshape. At the FEL intensities used here, significant photodepletion is observed so a logarithmic comparison of calculated intensity to the experimentally determined yield is used. A detailed assignment of the nitrobenzene vibrational fundamentals is done based upon comparison to previous literature and DFT calculations, as well as comparison to benzene vibrational modes. In order to ground the discussion, a DFT analysis of the infrared spectrum of the neutral is also undertaken. The neutral is well-characterized experimentally [58–61] and band assignments are generally well established; however, the current effort attempts to clarify and remedy minor discrepancies in the interpretation of the neutral spectrum in order to discuss the infrared spectrum of the anion in terms of that of the neutral.

As shown in Fig. 2, the scaled DFT calculations provide an effective model for both charge states. The lower panel of Fig. 2 shows the nitrobenzene neutral gas-phase infrared absorption spectrum from the NIST Chemistry Webbook overlaid on the DFT calculated frequencies convoluted with the same lineshape and scaling factor as used for the anion. The comparison of calculated and experimental vibrational frequencies is shown in Table 1. There are numerous experimental and computational studies of the vibrations of nitrobenzene, all of which are in overall agreement on the main features [58–62]. The experimental values for the nitrobenzene vibrations are taken from Clarkson et al. [59], except for two values noted which were left unassigned or are considered incorrectly assigned, in which case the values of Green and Harrison [58] are used. A scaling factor of 0.979 minimized the root-mean-square (rms) deviation between computed and experimental frequencies for both the anion and the neutral. For nitrobenzene, there is good overall agreement with experiment for the fundamental vibrational modes. The current computed vibrational frequencies also show close agreement with previous computational studies [59,62].

The major features in the IRMPD spectrum of the anion as listed in Table 1 are assigned based upon comparison with the DFT calculated spectrum. In addition to the present spectral data, a recent vibrational autodetachment study of nitrobenzene [17] revealed two unresolved C–H stretching bands at ~3050 and 3015 cm^{-1}; based upon the calculation these are assigned to modes ν_{2a} and ν_{26a}, respectively. For simplicity, the modes of the anion and neutral are numbered according to the Mulliken scheme. The nitrobenzene anion modes in Table 1 are shifted in order to allow for correspondence between like modes with the neutral within a given row. As seen in Fig. 2 and Table 1, all of the strongly infrared-active

Table 1
Vibrational frequencies of nitrobenzene neutral and anion according to experiment and scaled B3LYP/aug-cc-pVTZ harmonic frequency calculations.

Sym.	Neutral theory			FT-IR[b]		Anion theory			IRMPD		Matrix-IR[d]		Compare
	Mode (#)	Scaled[a] (cm^{-1})	IR int. (km/mol)	expt. (cm^{-1})	Δcalc. (%)	Mode (#)	Scaled[a] (cm^{-1})	IR int. (km/mol)	expt. (cm^{-1})	Δcalc. (%)	Expt. (cm^{-1})	Δcalc. (%)	Δexpts. (%)
A1	ν_1	3158	5	3107	−2	ν_{1a}	3147	2					
A1	ν_2	3130	8	3076	−2	ν_{2a}	3100	45	3050[c]				
A1	ν_3	3109	1	3049	−2	ν_{3a}	3062	6					
A1	ν_4	1594	3	1588	0	ν_{4a}	1580	95	1569	−0.7	1474.5[d]		
A1	ν_5	1482	10	1479	0	ν_{5a}	1466	2					
A1	ν_6	1340	276	1347	1	ν_{6a}	1347	212	1350	0.2	1365.7	1.4	1.1
A1	ν_7	1171	4	1174	0	ν_{7a}	1152	8	1156	0.3	1155.6	0.3	0.0
A1	ν_8	1094	33	1108	1	ν_{8a}	1066	188	1063	−0.3	1063.8	−0.2	0.1
A1	ν_9	1023	7	1020[b]	0	ν_{9a}	997	33	996	−0.1	1000.3	0.4	0.4
A1	ν_{10}	1002	0	1004	0	ν_{10a}	974	79	975	0.1	976.7	0.3	0.2
A1	ν_{11}	850	33	852	0	ν_{11a}	778	30	775	−0.4	781.2	0.4	0.8
A1	ν_{12}	681	8	681	0	ν_{12a}	641	0					
A1	ν_{13}	387	1	392	1	ν_{13a}	396	10					
A2	ν_{14}	986	0	990	0	ν_{14a}	950	0					
A2	ν_{15}	844	0	840	0	ν_{15a}	804	0					
A2	ν_{16}	409	0	417	2	ν_{16a}	434	0					
A2	ν_{17}	52	0	51	−2	ν_{17a}	111	0					
B1	ν_{18}	1003	0	990[b]	−1	ν_{18a}	948	1					
B1	ν_{19}	951	3	975	2	ν_{19a}	833	11	828	−0.6			
B1	ν_{20}	805	9	793	−1	ν_{20a}	715	32	707	−1.1	715.2	0.1	1.1
B1	ν_{21}	711	79	702	−1	ν_{22a}	558	29					
B1	ν_{22}	674	6	676	0	ν_{21a}	676	52	671	−0.7	674.5	−0.1	0.5
B1	ν_{23}	438	1	436	−1	ν_{23a}	385	0					
B1	ν_{24}	167	1	182	8	ν_{24a}	155	3					
B2	ν_{25}	3158	1	3107	−2	ν_{25a}	3146	7					
B2	ν_{26}	3122	9	3076	−1	ν_{26a}	3069	62	3015[c]				
B2	ν_{27}	1615	23	1620	0	ν_{27a}	1518	1					
B2	ν_{28}	1542	254	1523	−1	ν_{31a}	1267	133	1262	−0.4	1268.6	0.1	0.5
B2	ν_{29}	1459	1	1455	0	ν_{28a}	1445	3					
B2	ν_{30}	1323	13	1316	−1	ν_{29a}	1333	99	1337	0.3	1335.0	0.1	−0.1
B2	ν_{31}	1314	0	1308	0	ν_{30a}	1308	50	1309	0.1	1305.4	−0.2	−0.3
B2	ν_{32}	1160	1	1162	0	ν_{32a}	1130	5	1144	1.2			
B2	ν_{33}	1077	8	1070	−1	ν_{33a}	1055	16	1056	0.1	1054.4	−0.1	−0.2
B2	ν_{34}	613	0	611	0	ν_{34a}	615	0					
B2	ν_{35}	514	1	532	3	ν_{35a}	511	4					
B2	ν_{36}	251	1	255	1	ν_{36a}	245	1					
rms					**1.9**					**0.6**		**0.5**	**0.6**

[a] Hybrid DFT B3LYP/aug-cc-pVTZ harmonic frequencies are scaled by 0.979 for both neutral and anion.
[b] The FT-IR experimental values of Clarkson et al. (Ref. [59]) are used except for the two cases noted where the values of Green & Harrison (Ref. [58]) are used.
[c] The C–H stretching frequencies are taken from vibrational autodetachment study of Adams et al. (Ref. [17]).
[d] Matrix-IR experimental values from Ma et al. (Ref. [10]), experimental value for ν_4 of anion is disregarded.

fundamentals that are predicted in the spectral region studied are observed, and the intensities as well as frequencies of the B3LYP/aug-cc-pVTZ scaled harmonic frequency calculation agree with the experimental data. A satisfactory match to the observed spectrum could only be obtained when a relatively large basis set (aug-cc-pVTZ) was used. The slightly smaller basis sets of 6-311++G**, aug-cc-pVDZ, and 6-311++G(2d,2p) all resulted in significant deviation from experiment, particularly in modeling the bands in the 650–850 cm^{-1} range (Supplementary Information (S3)), demonstrating the importance of including sufficiently polarizable and diffuse basis sets for open-shell negative ions.

Two experimental bands are observed for the anion that are not predicted computationally: a band at 909 cm^{-1} and a band at 1532 cm^{-1}. The band at 1532 cm^{-1} could be due to the A_1 symmetry ring-CC stretch, but this is predicted to be much lower in frequency, at 1466 cm^{-1}. It could also be the B_2 symmetry mode predicted at 1518 cm^{-1}borrowing intensity from the higher frequency band. Also, it should be considered that in the neutral there is a Fermi resonance interaction between the B_2 symmetry fundamental at 1620 cm^{-1} and the B_2 symmetry $\nu_{10} + \nu_{34}$ combination band observed at 1606 cm^{-1} [59]. A similar situation for the anion would predict a band at ~1570 cm^{-1}. The band observed at 909 cm^{-1} could be the B_1 symmetry band with low intensity expected at 948 cm^{-1}. There are also numerous possibilities for combination bands, for instance it could be correlated with the $\nu_{12} + \nu_{36}$ combination band observed at 935 cm^{-1} in the neutral [59]; this gives a predicted value of 886 cm^{-1} for the anion.

The results of the current gas-phase IRMPD study can be compared to the results of a previous matrix-isolation IR absorption experiment by Ma and co-workers [10]. This serves to confirm and improve the spectral assignments as well as to provide a means for critical comparison of two experimental methodologies for the vibrational spectroscopy of a radical anion. As shown by Table 1, the major features of the matrix-isolation spectrum are reproduced by the IRMPD spectrum. Comparison of the matrix-IR spectrum [10] with the here-presented IRMPD spectrum and B3LYP/aug-cc-pVTZ computations resolves some issues with the previous assignment of the matrix-IR data which are likely due to the large discrepancy between the B3LYP calculations with the 6-311++G** basis and the aug-cc-pVTZ basis. In particular, the experimental peak at 674.5 cm^{-1} in the matrix spectrum was assigned to the B3LYP/6-311++G** computed B_1 symmetry mode at 695.2 cm^{-1} (unscaled) and the observed feature at 715.2 cm^{-1} was left unassigned. However, it is apparent from the B3LYP/aug-cc-pVTZ calculations that the 715.2 cm^{-1} feature is indeed a nitrobenzene anion absorption of B_1 symmetry, which corresponds to the band observed at 707 cm^{-1} in our IRMPD spectrum. The proper assignment of the observed matrix-IR peak at 674.5 cm^{-1} is to the B_1 symmetry peak that is calculated at 676.0 cm^{-1}(scaled aug-cc-pVTZ), which corresponds to the IRMPD peak at 671 cm^{-1}.

Furthermore, in light of the present IRMPD results and the new DFT calculations, it appears that the matrix-based assignment of the band at 1474.7 cm^{-1} is questionable. There is no significant IRMPD spectral activity seen for nitrobenzene in this region. Thus, we suspect that this relatively weak peak in the matrix spectrum does not arise from the nitrobenzene anion. A B3LYP/aug-cc-pVTZ calculation of anionic phenyl nitrite ($C_6H_5ONO^-$) suggests that it could be the carrier of the observed band, as it has a very strong IR absorption predicted at 1482 cm^{-1} (scaled by 0.979). However, this is at present only suggestive, as the other strong absorptions that could confirm this hypothesis are either out of the spectral range presented or obscured by a nitrobenzene neutral peak. Nonetheless, this absorption can be confidently excluded from the quantitative comparison between IRMPD and matrix spectra. In summary, the assignments based on the matrix spectrum are improved and two new experimental bands are revealed by IRMPD that are expected from the calculations: the band at 828 cm^{-1} and the band at 1144 cm^{-1}. Only a very small red-shift of 0.2% on average is apparent between the IRMPD and the matrix-isolation results.

As shown in Fig. 2, there is a significant difference between the spectra of the neutral and the anion of nitrobenzene. To investigate the band shifts within a common framework, the vibrational modes of the neutral and the anion are decomposed in terms of the component benzene vibrations. A computational method for projecting the normal modes of a molecule onto the normal modes of a similar basis molecule has been developed by Grafton and Wheeler in their fortran code named "ViPA', an abbreviation for vibrational projection analysis [55,56]. This technique was used to quantitatively determine the contribution of a given benzene normal mode in each normal mode of the neutral and anion of nitrobenzene. As shown in Table 2, this allows a direct comparison of the vibrational modes to benzene and to each other without a large degree of ambiguity. The procedure was confirmed by simple test cases and visual inspection, and results in a confident assignment of the nitrobenzene modes in terms of their benzene counterparts, as shown by the columns with the standard Wilson [63] notations for the normal modes of benzene. The description of the modes in terms of stretching (ν), bending (δ), or wagging (ω) is given according to the Herzberg notation [64]. The modes that are not easily described by a single benzene mode involve a strong perturbation from the nitro-group upon the phenyl ring or are strongly localized on the nitro group. The arrangement of the neutral and anion within given rows of Table 2 for comparison of vibrational modes of each is based upon the projection onto the benzene framework, and not necessarily (although usually) upon similarity of the movement of the substituent functional group.

The qualitative degree of agreement between the nitrobenzene modes and the benzene normal modes given in the left-most columns is based upon the quantitative degree of agreement described under the heading of 'ViPA mix'. The relevant benzene modes are listed, with the percentage of the most dominant mode given under the heading 'max.', and the degree of the mode to not be representable as a benzene normal mode given under the heading 'def.' (deficiency). Benzene modes of minor importance in describing the nitrobenzene mode are given in parentheses, and involve a contribution of less than 10%. Thus, a quick glance at the number of modes listed and the size of the deficiency gives a good impression of the degree of perturbation of the nitro group on the phenyl ring and the localization of the vibration on the nitro group. Of course only modes within the same C_{2v} symmetry type can be mixed. It is quite clear for instance, which modes are due to NO_2 stretches, and the degree of coupling to ring modes is immediately obvious. Since the coupling of the $-NO_2$ group vibrations to the ring is strong in certain cases, the assignments of nitrobenzene normal modes to component benzene vibrations shows some discrepancies between previous studies [59,61,62] that the current study quantitatively clarifies.

By grounding the nitrobenzene vibrational modes of the neutral and anion in the benzene basis, we can look directly at the influence of electron attachment upon each individual vibrational mode. Certain trends are apparent for both the neutral and the anion: the benzene C–H stretching modes are coupled strongly to each other by the addition of a substituent, but only slightly to other modes. The A_2 symmetry C–H bending modes are left essentially unperturbed, and the benzene C–C stretching and C–H wagging modes are more strongly perturbed by the substituent. Finally, with this analysis in mind, a subsequent projection is even more clarifying. Shown in the right-side of Table 2 is a projection of the nitrobenzene anion vibrational modes onto the neutral modes as a basis. This directly reveals the effect of electron attachment upon the vibrations of nitrobenzene, and the benzene components provide a framework for describing these changes. The numbers

Table 2
Vibrational modes of nitrobenzene neutral and anion described in terms of benzene modes and account of band shifts in the anion in terms of the nitrobenzene neutral modes.

Description			Nitrobenzene neutral vibrational modes						Nitrobenzene anion vibrational modes					Compare nitrobenzene neutral vs. anion				
Sym. C_{2v}	Benzene Wilson[a]		#	freq. cm^{-1}	Mode description Herzberg[b]	Benzene basis ViPA[c] mix	max. %	def. %	#	freq. cm^{-1}	Benzene basis ViPA[c] mix	max. %	def. %	Neutral basis ViPA[c] mix	max. %	Differences	$\Delta\nu$ cm^{-1}	$\Delta\nu$ %
A_1	s	2	ν_1	3226	νCH	2,13,7a,(20a)	49	0	ν_{1a}	3214	2,13,7a,20a	44	0	1	99	–	−12	0
A_1	s	20a	ν_2	3197	νCH	20a,2,(13)	57	0	ν_{2a}	3166	20a,2,7a	53	0	2,3	84	–	−31	−1
A_1	s	13	ν_3	3176	νCH	13,7a	55	0	ν_{3a}	3128	13,7a,2	57	0	3,2	84	–	−48	−2
A_1	t	8a	ν_4	1628	νCC	8a	100	0	ν_{4a}	1614	8a	96	0	4,(6)	96	–	−14	−1
A_1	t,α	19a	ν_5	1514	νCC	19a	99	0	ν_{5a}	1497	19a,(20a)	87	0	5,(6)	91	–	−17	−1
A_1	–	–	ν_6	1368	$\nu_{sym}NO_2$ + νCH	20a,7a,(2,13)	17	47	ν_{6a}	1376	7a,20a,19a,13,2	21	11	6,8,(5)	59	νCN + νCC	258	19
A_1	β	9a	ν_7	1196	δCH	9a	92	1	ν_{7a}	1177	9a,(1,18a)	87	5	7,(6)	96	–	−19	−2
A_1	–	–	ν_8	1118	νCC+δCH+δCC+ νCN	1,18a,12,(9a)	28	8	ν_{8a}	1089	12,9a,1,(18a)	43	24	8,6,(10)	64	$\nu_{sym}NO_2$	−279	−25
A_1	β	18a	ν_9	1045	δCH	18a,12,1	70	0	ν_{9a}	1018	18a,1	75	0	9,(10)	94	–	−27	−3
A_1	αt	12,1	ν_{10}	1024	δCC+ νCC	12,1	56	0	ν_{10a}	995	1,12	47	2	10,(8,9)	86	–	−29	−3
A_1	–	–	ν_{11}	868	δNO_2	(1,12,7a,18a)	8	58	ν_{11a}	795	6a,1	22	48	11,12	83	$-\delta NO_2$	−73	−8
A_1	α	6a	ν_{12}	696	δCC + δ NO_2	6a	78	20	ν_{12a}	655	6a	52	44	12,11,(8)	86	$+\delta NO_2$	−41	−6
A_1	–	–	ν_{13}	395	ν(C–NO2)+ δCC	6a,(7a,1)	15	72	ν_{13a}	404	6a,(7a)	20	72	13,(11)	99	–	9	2
A_2	γ	17a	ν_{14}	1007	ωCH	17a	100	0	ν_{14a}	970	17a	100	0	14	100	–	−37	−4
A_2	γ	10a	ν_{15}	862	ωCH	10a	100	0	ν_{15a}	821	10a	100	0	15	100	–	−41	−5
A_2	δ	16a	ν_{16}	418	ω(C–C–C)	16a	100	0	ν_{16a}	443	16a	99	0	16	100	–	25	6
A_2	–	–	ν_{17}	53	NO_2 torsion	–	0	100	ν_{17a}	113	–	0	100	17	100	–	60	112
B_1	γ	5	ν_{18}	1025	ωCH	5,17b	78	0	ν_{18a}	968	5,10b,(17b)	82	0	18,19,(20)	87	–	−57	−6
B_1	γ	17b	ν_{19}	972	ωCH	17b,10b,5	58	0	ν_{19a}	851	17b,10b	75	0	19,(18,21,20)	87	–	−121	−12
B_1	γ	10b	ν_{20}	822	ωCH + ωNO_2	10b,15,(5)	66	5	ν_{20a}	730	10b,4,11	48	1	20,22,(21,18)	73	$-\omega NO_2$	−92	−11
B_1	γ	11	ν_{21}	726	ωCH + ωNO_2	11,(4,17b)	86	8	ν_{22a}	570	11,10b,4,17b	35	8	21,20,22,(23)	60	$+\omega NO_2$	−156	−21
B_1	δ	4	ν_{22}	688	ω(C–C–C)	4	92	1	ν_{21a}	690	4,11	51	0	22,21,(20)	71	+ωCH	2	0
B_1	δ	16b	ν_{23}	448	ω(C–C–C)	16b,(11)	92	6	ν_{23a}	393	16b,(17b)	81	13	23,(20,22,21)	91	–	−55	−12
B_1	–	–	ν_{24}	170	ωNO_2	(16b,11,10b)	6	91	ν_{24a}	158	(16b,11,10b)	9	89	24	100	–	−12	−7
B_2	s	20b	ν_{25}	3226	νCH	20b,7b	66	0	ν_{25a}	3213	20b,7b	61	0	25	100	–	−13	0
B_2	s	7b	ν_{26}	3189	νCH	7b,20b	66	0	ν_{26a}	3135	7b,20b	61	0	26	100	–	−54	−2
B_2	t	8b	ν_{27}	1650	νCC	8b	95	3	ν_{27a}	1551	8b	94	0	27,(28)	89	–	−99	−6
B_2	–	–	ν_{28}	1575	$\nu_{asym}NO_2$ + νCC	19b,9b,(15,18)	26	29	ν_{31a}	1294	9b,15,18b	39	22	28,31,30,29	38	$-\nu_{asym}NO_2$	−281	−18
B_2	t,α	19b	ν_{29}	1491	νCC	19b,3,(9b)	67	3	ν_{28a}	1476	19b,(3,14)	84	0	29,(28,30)	80	–	−15	−1
B_2	t,α	14	ν_{30}	1351	νCC	14	92	1	ν_{29a}	1362	14,(19b,3)	86	4	30,28	75	$+\nu_{asym}NO_2$	11	1
B_2	β	3	ν_{31}	1342	δCH	3,9b,(14,18b)	73	1	ν_{30a}	1336	3,(14,19b)	81	7	31,28	64	$+\nu_{asym}NO_2$	−6	0
B_2	β	15	ν_{32}	1185	δCH	15,9b	64	0	ν_{32a}	1154	15,9b	68	0	32	98	–	−31	−3
B_2	β	18b	ν_{33}	1100	δCH	18b,15,9b	71	1	ν_{33a}	1078	18b,9b	75	1	33	97	–	−22	−2
B_2	α	6b	ν_{34}	626	δCC	6b	98	1	ν_{34a}	628	6b	99	1	34	100	–	2	0
B_2	–	–	ν_{35}	525	NO2 rocking	(9b,18b,15)	9	75	ν_{35a}	522	(9b,18b,.15)	9	76	35	100	–	−3	−1
B_2	–	–	ν_{36}	257	δ(C–NO2)	(6b,18b)	1	98	ν_{36a}	250	(6b)	1	99	36	100	–	−7	−3

[a] Ref [63].
[b] Ref [64].
[c] Ref [55,56].

listed under 'ViPA mix' for the 'neutral basis' refer to the Mulliken numbering scheme of the neutral vibrational modes. There is no 'deficiency' column listed because the modes of the neutral in total provide a complete basis for the anion vibrational modes. It is clear from inspection what vibrational modes of nitrobenzene are strongly perturbed by electron attachment, thus, the difference in the ground state potential surface between the anion and neutral is not only apparent in the frequency shifts, but also in the mode character. The comments listed under 'differences' describe the cases of strong change in the character of the vibrational mode of the anion relative to the neutral in terms of the NO_2 functional group or a component of the ring vibrations.

While for the most part the nitrobenzene neutral and anion modes are quite similar, some of the more striking shifts in the anion observed include a reversal of the order of the NO_2 symmetric stretch frequency and the CN stretch frequency, a change in the interaction of the NO_2 'umbrella'-type motion with the C–H wagging modes, and an increase in the degree of coupling of the NO_2 antisymmetric stretching frequency with vibrations of the phenyl ring. The structures shown in Scheme 1 provide a useful means for interpreting the spectral shifts observed, particularly keeping in mind resonance structure (5). For instance, the NO_2 torsion mode frequency (ν_{17} in neutral and anion) is more than doubled in the anion, as would be expected from increased CN π-bonding. Aside from this mode, the modes which map the anion to the neutral without a large degree of mixing are relatively close in frequency; on the other hand, modes which do change frequency to a large degree involve a significant change in the relative mode characters.

One of the most dramatic changes in the anion is the switch in magnitude between the CN stretching frequency and the NO_2 symmetric stretching frequency. The CN stretch in the neutral is strongly mixed with the ring vibrations, as shown by the many benzene components in the neutral ν_8 mode and the small deficiency factor. The NO_2 symmetric stretching mode in the neutral (ν_6) is not as strongly mixed, coupling only to the C–H stretching modes. Upon electron attachment, the dominant benzene modes that couple to the CN stretch and to the NO_2 symmetric stretch flip, since the CN stretching frequency in the anion (ν_{6a}) shifts up out of range of the ring C–H bending modes and closer to the frequency of the CC stretching modes; the NO_2 symmetric stretch frequency (ν_{8a}) simultaneously shifts down into the range of the C–H bending modes. The coupling to the benzene modes changes dramatically for these two vibrations since the NO bonds weaken and the CN bond tightens to produce a ≈25% decrease in the NO_2 symmetric stretch frequency and a ≈20% increase in the CN stretch frequency. These motions also become more coupled to each other in the anion as compared to the neutral, and this fact is likely responsible for the shift of infrared intensities in the anion observed in the experiment and listed in Table 1 for these modes.

Another interesting shift in the anion concerns the B_1 symmetry modes, in particular the change in the coupling of the NO_2 out-of-plane deformation 'umbrella' type mode. In the neutral, this local mode is coupled to both of the benzene C–H out-of-plane modes as seen by the deficiency factor in modes ν_{20} and ν_{21}. In the anion this vibration shifts down in frequency due to the decrease in shared π-bonding in the ONO system, and hence the umbrella motion couples more strongly to the lower frequency benzene C–H out-of-plane bending mode. Thus mode ν_{22a} shows a deficiency factor while mode ν_{20a} does not. Another interesting difference in the modes of this symmetry is the effect the substituent has on the coupling of the phenyl ring C–C–C out-of-plane bending modes to the C–H out-of-plane bending modes. While for neutral mode ν_{22} the out-of-plane ring bending is not coupled to the C–H bending modes, this mode in the anion (i.e. ν_{21a}) couples these two motions, presumably by raising the frequency of one of the C–C–C bending modes to be closer to the frequency of the C–H out-of-plane bending modes, and lowering the frequency of the other C–C–C bending mode, ν_{23a}.

Table 3
Calculated electronic charge distribution in nitrobenzene neutral and anion according to natural population analysis (npa) method at B3LYP/aug-cc-pVTZ level of theory.

Position	Atom	Neutral	Anion	Difference	%Diff.	Adj. diff.
Substituent	N	0.50	0.35	−0.16	−45	−0.08
	O	−0.37	−0.58	−0.21	−36	−0.14
	O	−0.37	−0.58	−0.21	−36	−0.14
	C1	0.04	0.06	0.02	+42	0.09
Ortho	C2	−0.18	−0.24	−0.06	−24	0.01
	C6	−0.18	−0.24	−0.06	−24	0.01
	H	0.24	0.22	−0.02	−9	0.05
	H	0.24	0.22	−0.02	−9	0.05
Meta	C3	−0.19	−0.22	−0.03	−13	0.04
	C5	−0.19	−0.22	−0.03	−13	0.04
	H	0.21	0.18	−0.03	−19	0.04
	H	0.21	0.18	−0.03	−19	0.04
Para	C4	−0.17	−0.29	−0.13	−43	−0.06
	H	0.21	0.18	−0.03	−18	0.04
Charge distribution						
Total		0	−1	−1		0
$-NO_2$		−0.24	−0.82	−0.58		−0.36
Ring		0.24	−0.18	−0.42		0.36

As the NO_2 symmetric stretch is red-shifted in the anion due to the weakening of the NO bond as predicted by resonance structure (5), it is expected that the antisymmetric stretch red-shifts as well. This is indeed observed and moreover the ≈20% red-shift of the antisymmetric NO_2 stretching mode (ν_{28} in the neutral and ν_{31a} in the anion) results in a large degree of mixing with the phenyl ring in-plane CH bending for the anion which is not present in the neutral. This is further evidenced by the higher deficiency factor for the ν_{29a} and ν_{30a} modes compared to the correlated modes in the neutral. The result of this coupling is to distribute infrared intensity over these three modes in the anion, whereas it was essentially confined to a single mode in the neutral (Fig. 2 and Table 1).

3.2. DFT computations of nitrobenzene bonding characteristics

The good agreement between computed and experimental spectra lends some confidence to the use of DFT computations for other properties, such as charge density and internal rotation barriers. The agreement of the observed vibrational shifts with the suggested importance of resonance structure (5) can be further investigated by these computations. In particular, resonance structures (3–5) shown in Scheme 1 each suggest specific molecular orbital shapes and charge distributions that can be computationally investigated. The graphical representation of the LUMO of the neutral and HOMO of the anion from B3LYP/6-311++G** calculations shown in the work of Ma et al. [10] agrees with the current results from B3LYP/aug-cc-PVTZ calculations (Supplementary Information (S4)). The molecular orbital clearly shows anti-bonding character for the NO π-bonds and bonding character for the CN π-bonds. In addition, there is bonding character between the ortho- and meta-position carbons and anti-bonding character between the meta- and para-position carbons, with molecular orbital density isolated on the para-position carbon. All of these characteristics indicate the predominance of the distonic resonance structure (5).

To further examine these characteristics, the charge density of the individual atoms can be computed directly according to the natural population density method within Gaussian03 [54], using the same level of theory as employed for the harmonic vibrational frequencies calculation. The results of these computations are summarized in Table 3, and indicate a strong difference in the charge densities between the neutral and anion. The neutral obviously places a strong partial positive charge on the nitrogen

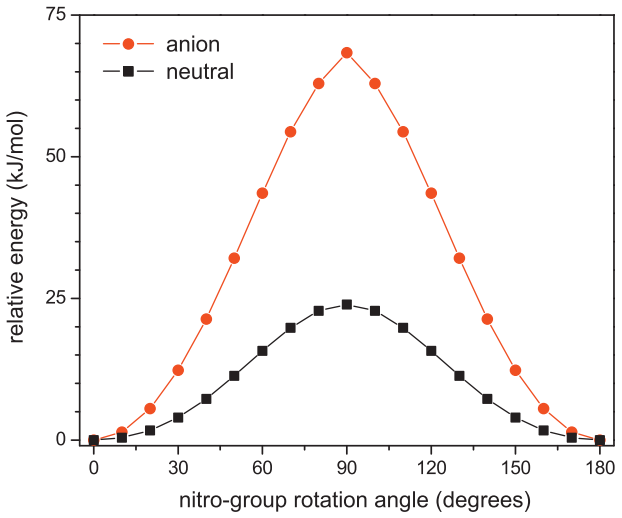

Fig. 3. Calculated energies for internal rotation of the nitro group at B3LYP/6-311++G(2d,2p) level of theory for nitrobenzene neutral and anion. The *x*-axis corresponds to the angle of the N–C–C axis relative to the C–N–O axis, and is only shown from 0 to 180° due to molecular symmetry. Note the significantly higher barrier to rotation in the anion, indicative of increased CN π-bonding.

atom, and a relatively small partial negative charge on the ring carbons, with a slightly more negative charge at the meta-position. This distribution agrees with the neutral resonance structure (1) of Scheme 1, certainly does not agree with resonance structure (2), and is a classic example of the meta-directing deactivation towards electrophilic aromatic substitution dominated by inductive effects. The situation for the anion is quite different, with the para- and ortho-position carbons showing greater charge density than the meta-position, and the nitrogen and oxygen partial charges showing a greater disparity in the sign of the charge. The absolute differences between the partial charges show "where" the excess charge of the added electron has gone; it is clear that the $-NO_2$ group has received a greater portion of the excess charge than the ring. The percentage difference is striking for the para-position carbon, and the overall shifts are evocative of the para-directing electrophilic aromatic substitution activation effect due to strong resonance interactions with a substituent. The final column of Table 3 under the heading 'adj. diff.' shows the result of removing the excess charge from the anion equally from each atom, to directly compare the relative shift of the charge within the molecule. This 'adjusted difference' reveals a greater localization of the negative partial charge on the nitro group, and significantly more so for the oxygen atoms than for the nitrogen atom. There is a clear shift in the electron density towards the para-position carbon and a shift of electron density away from the meta-position carbon due to the increased importance of resonance interaction between the nitro group and the ring in the anion relative to the neutral.

The large increase of the torsional vibrational frequency of the NO_2 group in the anion relative to the neutral is also suggestive of CN π-bond character, and this should result in a larger barrier to internal rotation in the anion as compared to the neutral. Fig. 3 shows the results of a relaxed potential energy surface scan performed by optimization of all molecular parameters while fixing the ring-NO bond angle. The B3LYP/6-311++G(2d,2p) computed barrier height for the nitrobenzene neutral is 23.9 kJ/mol and is in rough agreement with experimental values (>13.6 kJ/mol [65] and 19 kJ/mol [66]) as well as previous MP2 computations (19–25 kJ/mol [67]). As shown in Fig. 3, at the same level of theory, the barrier for internal rotation in the anion is calculated to be much higher, 68.3 kJ/mol. The accuracy of the DFT calculations towards modeling the neutral internal rotation is sufficient to suggest that this increased barrier calculated for the anion is reliable and thus provides further evidence for the importance of the π-resonance interaction between the nitro and ring moieties.

3.3. Energetics and dynamics

To aid in the interpretation of the various unimolecular decomposition channels observed, the relative energies of the processes are considered. Experimental values for the key reactions of interest are available and are compared to values calculated by various methods in Table 4. As shown in the table, the preponderance of resonant electron detachment over NO_2^- dissociation is commensurate with the respective order of the 1.0 eV detachment [2] and 1.8 eV dissociation [14] energies. The fact that the $C_6H_5^-$ fragment formed via NO_2 neutral loss is not observed is also easily rationalized considering the significantly higher energy for this reaction as compared to the two observed processes. Other possible decomposition channels not listed in the table and not observed in this experiment include O^- loss, which is observed in dissociative electron attachment [14] but is highly endothermic (3 eV), and the isomerization/dissociation process of NO loss to form the phenoxide ion, $C_6H_5O^-$. While this latter process is actually exothermic by 0.6 eV (according to B3LYP calculations using the aug-cc-pVTZ and 6-311++G** [10] basis sets), the transition state required for its formation is highly endothermic (computed at 2.8 eV by the same level of theory [10]). Thus, the current observation of only electron loss and NO_2^- loss is reasonable considering the significantly higher energy barriers to all other processes.

The relative success of the DFT calculation towards modeling the potential energy surfaces of the neutral and anion does not necessarily translate to success in calculating their relative energies, as the electron affinities of radical anions can be difficult to compute accurately. The calculated energy of electron loss (detachment) from the anion is compared to experimental values for the adiabatic electron affinity (AEA) and the vertical detachment energy (VDE) in Table 4. There is a discrepancy of ≈0.3 eV between the experimental and DFT-computed values that is not strongly mitigated by increasing the size of the basis set. However, the relative difference between the AEA and VDE matches the experimental value since this is a property related to the displacement of atom positions in the neutral, a property that the DFT calculations do successfully model. This is not an unfamiliar result, as examples of a similar effect have been observed for the SF_6^- anion, where the DFT vibrational frequencies give a good match to experiment [37] but significantly overestimate the stability of the anion [68]. As was demonstrated for SF_6^- [69,70], coupled-cluster calculations can be expected to give a more accurate value for the electron affinity, provided a basis set of sufficient size is employed. This expected result was not achieved in the current study; as is apparent from the result in Table 4, the coupled-cluster CCSD(T)/6-311++G** single point energy calculations performed at the B3LYP/aug-cc-pVTZ optimized geometries suffer from basis-set deficiency. This relatively small basis set can be expected to "constrict" the anion more severely than the neutral, thus artificially raising the energy of the anion and lowering the computed adiabatic electron affinity. To better assess this effect, the computed electron affinities for two of the components of the nitrobenzene anion, the phenyl and nitro group, are also presented in Table 4. The DFT AEA computations show a reasonable agreement to the experimental values for the NO_2 and C_6H_5 molecules. However, the CCSD(T) computed AEA for NO_2 significantly deviates from the established experimental value, while giving reasonable agreement for the experimental C_6H_5 AEA. Thus, it appears that a large part of the failure of the coupled-cluster calculations to accurately compute the nitrobenzene AEA is due to poor modeling of the nitro moiety.

Table 4
Calculated and experimental energies of selected unimolecular decomposition reactions of nitrobenzene anion, parent neutral, and relevant dissociation fragments presented in units of eV.

Calculation method	Dissoc. NO_2^- loss	Dissoc. NO_2 loss	Detach. AEA	Detach. VDE	NO_2 AEA	C_6H_5 AEA	$C_6H_5NO_2$ NO_2 loss
B3LYP/							
6-311++G**	1.84	3.07	1.31	1.61			
aug-cc-pVDZ	1.88	3.09	1.29	1.58			
6-311++G(2d,2p)	1.88	3.08	1.28	1.58	2.28	1.07	2.88
aug-cc-pVTZ	1.84	3.03	1.25	1.57	2.25	1.06	2.83
CCSD(T)/[a]							
6-311++G**	1.79	2.72	0.65	0.91	2.02	1.09	3.16
Experiment							
Desfrancois et al. [2]			1.00	~1.3			
Pelc et al. [14]	1.8[b]						
Ervin et al. [1]					2.273		
Gunion et al. [3]						1.096	
$\Delta_f H^\circ$ [71,72]							3.10[c]
$\Delta_f H^\circ$		3.00[d]					

[a] Results presented for the CCSD(T) method were single-point energy calculations using the B3LYP/aug-cc-pVTZ optimized structures.
[b] The experimental value for NO_2^- loss is determined by combining the 0.8 eV appearance energy from Ref. [14] with the AEA from Ref. [2].
[c] The experimental value for NO_2 loss from neutral nitrobenzene is determined by using the heats of formation of $C_6H_5NO_2$ (Ref.[71]), NO_2 (Ref.[71]) and C_6H_5 (Ref. [72]).
[d] The experimental value for NO_2 loss from the anion is determined from the experimental value of NO_2 loss from the neutral and the experimental adiabatic electron affinities of $C_6H_5NO_2$ and C_6H_5.

In order to further assess the accuracy of the selected computational methods, the calculated energies of dissociation by NO_2 and NO_2^- loss from the nitrobenzene anion are also presented in Table 4, as is the energy of NO_2 loss from the parent neutral. The computed results are compared to experimentally derived values. The experimental value for the NO_2^- loss from the anion is determined by combining the 0.8 eV appearance energy for NO_2^- from dissociative electron attachment [14] with the experimental electron affinity of the nitrobenzene molecule [2]. The experimental value for NO_2 loss from the neutral is determined by using the heats of formation of the various components: $C_6H_5NO_2\,\Delta_f H^\circ = 87.65$ kJ/mol [71], $NO_2\,\Delta_f H^\circ = 35.94$ kJ/mol [71], and $C_6H_5\,\Delta_f H^\circ = 350.6$ kJ/mol [72]. The NO_2 loss energy from nitrobenzene has been calculated by previous ab initio [73] and DFT [74] computations, and showed reasonable agreement to this experimental value. The energy of this same process in the anion is related to that of the neutral by the difference in electron affinities between the nitrobenzene and phenyl molecules. It is apparent that the significantly lowered dissociation of the anion via NO_2^- loss compared to NO_2 loss is due to the much higher electron affinity of NO_2 as compared to C_6H_5.

The computed values for NO_2^- dissociation agree reasonably well with the experimental values for all of the methods employed but upon inspection it is apparent that this is due in part to a cancellation of errors. The DFT computations produce a bond dissociation energy of the neutral that is lower than experiment and an electron affinity of nitrobenzene that is greater than that of phenyl. The result of overvaluing the parent anion stability and undervaluing the "inherent" bond strength of the neutral results in a cancellation to produce an NO_2^- loss energy that is in rough agreement with experiment. For the coupled-cluster calculations the situation is different but the result is the same; in this case the bond dissociation of the neutral is calculated in closer agreement with experiment, and the electron affinities of both the parent and NO_2 fragment are nearly equally too small, resulting in a cancellation of this energy difference and producing an NO_2^- loss energy in agreement with experiment. While the cancellation of errors for the DFT calculations also produce an NO_2 neutral loss energy from the anion in agreement with experiment, the coupled-cluster calculations do not compute the phenyl AEA to be too low, and thus the cancellation of errors does not hold for NO_2 neutral loss from the anion, resulting in a lower calculated energy than observed. While it is likely that improvement in computational accuracy for the dissociation and detachment processes can be expected from the use of larger basis sets, the use of single-reference computational methods such as DFT and CCSD(T) is not ideal since the electronic wavefunction of the radical anion is likely to have significant multi-reference character. However, improvement by the use of multi-reference methods is beyond the scope of the current study. Overall, while the calculations are not of sufficient quality to be considered highly quantitatively accurate, they do show a satisfactory qualitative agreement with experiments and establish a clear trend in the energetic order of the relevant unimolecular processes.

The large yield difference in the photo-induced processes can be further interpreted in terms of kinetic considerations within the framework of statistical models of unimolecular dissociation. As discussed in many reviews [43,75], since the decomposition energy is much higher than the energy of the individual photons absorbed, intramolecular vibrational redistribution of energy (IVR) distributes the input energy into the bath of available states before photodecomposition; since the molecule has a sufficiently large numbers of anharmonically coupled oscillators the rate of the decomposition is slow compared to the IVR randomization. Thus statistical models of unimolecular decomposition can be expected to be appropriate to model both the electron detachment and dissociation processes. Nitrobenzene has been demonstrated to randomize input energy sufficiently quickly and thoroughly such that upon isolated gas-phase attachment of low-energy electrons, the autodetachment of the electron is delayed by a significant time, measured in the range of tens of μs[12,15] to ms[11], despite the fact that the anion has an internal energy above the detachment threshold. Many theoretical approaches have been developed to model this phenomenon in this and other metastable negative ions; one of the earliest [76–78] and conceptually simplest models is referred to as quasi-equilibrium theory (QET), which is a statistical model of unimolecular decomposition based upon detailed balancing. There are numerous examples of the application of QET methods to negative ion dynamics [12,16,79] and a discussion is given in a recent review[46]. A recent implementation of the theory for the modeling of the temperature dependence of the lifetimes of metastable negative ions of SF_6 and C_6F_6[80], as well as C_2Cl_4[81], showed some success accounting for the observed experimental results, despite lacking the detail of more sophisticated statistical

models[82]. Considering the fundamental property of unimolecular statistical models that the activated species has no 'memory' of the activation process, it follows that the QET model applied to the temperature dependence of negative ion lifetimes is appropriate for determination of detachment rates of negative ions undergoing multiple-photon IR absorption.

A detailed explanation of the method used in the current work can be found in the SF_6^- and $C_6F_6^-$ study [80]. Briefly, a QET detachment model employs a microscopic equilibrium between the electron attachment and detachment processes, such that the product of the density of states for each system and its interconversion rate are equivalent, as shown in Eq. (1):

$$k_{att}(E_e, E_{neut})\,\rho_{product}(E_e, E_{neut}, \upsilon_{neut}) = k_{det}\rho_{anion}(E_{anion}, \upsilon_{anion}). \quad (1)$$

The rate of the detachment process (k_{det}) is thus determined by the electron attachment rate (k_{att}), the density of states of the neutral and free-electron product system ($\rho_{product}$), and the density of states of the activated anion (ρ_{anion}). The electron attachment rate (k_{att}) can be determined by a thermally averaged representative rate, or alternatively, is given as a function of energy by the product of the velocity-dependent electron-capture cross-section (σ_e) with the electron velocity (v_e). Since the electron-capture cross-section and the densities of states are energy-dependent, the detachment rate is a function of the partitioning of available energy between the internal energy of the neutral (E_{neut}) and the translational energy of the electron (E_e). The available energy to the product system is the energy of the activated anion (E_{anion}) minus the adiabatic electron affinity (AEA):

$$E_e + E_{neut} = E_{anion} - AEA. \quad (2)$$

As discussed in the previous model of SF_6^- detachment, the density of the states of the product system is given by the derivative of the product of the sum of states of the free electron (G_e) and the neutral molecule (G_{neut}):

$$\rho_{product} = \frac{d}{dE}G_{product} = \frac{d}{dE}G_eG_{neut} = \rho_eG_{neut} + G_e\rho_{neut}. \quad (3)$$

For typical energy distributions of E_e and E_{neut} the dominant term in the sum of Eq. (3) is the term containing the density of states of the free electron:

$$\rho_eG_{neut} \gg G_e\rho_{neut}, \quad (4)$$

thus

$$\rho_{product} \approx \rho_eG_{neut} \quad (5)$$

and finally the familiar expression for a unimolecular decomposition process is obtained:

$$k_{det} = \frac{\sigma_e(E_e)\,v_e(E_e)\,\rho_e(E_e)\,G_{neut}(E_{neut}, \upsilon_{neut})}{\rho_{anion}(E_{anion}, \upsilon_{anion})}. \quad (6)$$

Thus, a variety of empirical factors are required for the detachment model: the electron velocity-dependent electron-capture cross-section, the outgoing electron energy, the vibrational frequencies of the neutral and anion, and the energy difference between the two states. The low-energy electron-capture cross-section is well-characterized for nitrobenzene [12,14], as is the electron affinity [2], and the current study provides a good analysis of the vibrational frequencies of the two states. Thus the needed parameters for the model are available provided a reasonable assumption about the partitioning of energy in the product system is made. There is both experimental evidence and theory to support a distribution of relatively low kinetic energy ejected electrons in this experiment. The SF_6 electron scavenger gas employed has a very high cross-section for dissociative electron attachment forming SF_5^- at electron energies above 0.2 eV, yet no SF_5^- signal is observed under our experimental conditions despite large SF_6^- signals. This implies the energy of the photo-ejected electrons is well below 0.2 eV. A further consideration comes from the work of Troe et al. [82], where a detailed analysis of various statistical models of the thermionic emission from SF_6^- showed a distribution of electron energies peaked at 0.01 eV near threshold and peaked well below 0.1 eV for electrons emitted from ions with an internal energy of 1 eV above threshold. Thus, given these constraints, it is not unreasonable to assume a single representative ejected electron energy of 0.01 eV.

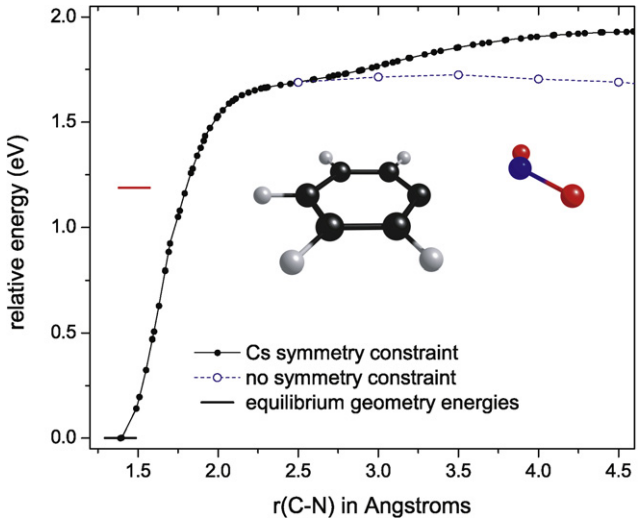

Fig. 4. Relaxed potential energy surface scan of C–N bond length in the nitrobenzene anion calculated at B3LYP/6-311++G(2d,2p) level of theory. The energies are determined by optimizing all molecular parameters but the fixed bond length. The calculated zero-Kelvin thermodynamic NO_2^- dissociation energy is 1.8 eV, and the calculated energies of the optimized anion (0 eV) and neutral (1.2 eV) are marked by the thick horizontal lines. As shown by the dotted line, at a C–N bond length near 2.5 Å there is a saddle point with an energy decrease towards an angle from the plane of symmetry containing the C–N bond. The structure shown in the image is the result of a partial optimization with a fixed C–N bond of 2.5 Å that is used as a model for the dissociation transition state.

The use of statistical models for calculation of unimolecular dissociation rates has a long history [83] and is well reviewed [84]. In the simplest formulation, the microcanonical dissociation rate (k_{diss}) is proportional to a ratio of the vibrational sum of states of a molecular configuration representing the proposed transition state (G_{TS}) and the vibrational density of states of the activated parent molecule (ρ_{parent}) with an internal energy E^*, as shown in Eq. (7):

$$k_{diss}\frac{G_{TS}(E^* - E_{TS}, \upsilon_{TS})}{h\rho_{parent}(E^*, \upsilon_{parent})}.$$

The vibrational sum of states of the transition state requires knowledge of the real vibrational frequencies of this state (ν_{TS}) excluding one imaginary frequency correlating to the reaction coordinate as well as the energy difference of the state with respect to the parent molecule (E_{TS}). To determine a suitable approximation for this transition state with regard to NO_2^- loss from nitrobenzene, a relaxed potential energy surface calculation was performed by optimizing all molecular parameters at fixed lengths of the CN bond. The results of these B3LYP/6-311++G(2d,2p) calculations are shown in Fig. 4, along with the computed energies of the vibrational ground states of the neutral (i.e. the computed adiabatic electron affinity of 1.2 eV) and anion at the same level of theory. The dissociation energy tends towards the thermodynamic calculated limit of 1.8 eV at long CN bond lengths when the system is constrained to C_s symmetry by a plane containing the CN bond. The lower energy dissociation path shown is a result of an anion complexation

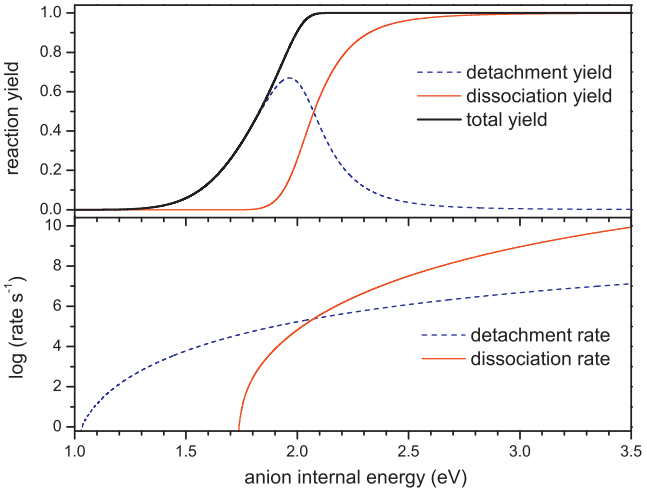

Fig. 5. Detachment and dissociation rates and combined yields from microcanonical statistical models. See text for model parameters. Shown in the lower panel is the log of the microcanonical rate constants as a function of total energy in the anion. The upper panel shows the yield of the respective channels independently and the combined yield combined assuming a 10 μs detection window. The threshold for detachment to thermal neutral molecules and low-energy electrons is at ~1.1 eV, the threshold for dissociation to thermal NO_2^- and C_6H_5 products is 1.73 eV.

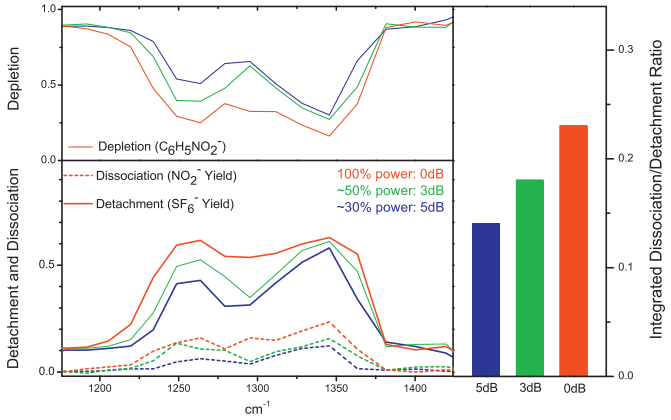

Fig. 6. Low resolution IRMPD spectrum of nitrobenzene anion via depletion, detachment and dissociation channels acquired at different laser intensities. The laser power is adjusted to levels of 100% (0 dB), 50% (3 dB) and 33% (5 dB), and the lowest power is closest to the conditions by which the spectrum in Fig. 1 is acquired. The panel at right shows the ratio of the integrated yields of the dissociation and detachment processes over the frequency domain shown at each of the three laser powers. Upon inspection of the peak at 1350 cm^{-1}, the dotted line shows the dissociation channel becomes increasingly relevant as the yield limit predicted by the model (shown in the upper panel of Fig. 5) is reached for the detachment channel.

energy that is gained when the NO_2^- group is allowed to interact with the ortho- and meta-positions of the C_6H_5 molecule. From examination of the structures and energy, it was determined that a structure at a CN bond distance of 2.5 Å provides a good approximation to a transition state for the system, as the energy of the state is clearly near the dissociation threshold, and the potential energy surface provides a clear imaginary frequency along the association/dissociation pathway. Thus, as shown by the structure in Fig. 4 (the coordinates and harmonic vibrational frequencies are provided in Supplementary Information (S5)), a B3LYP/aug-cc-pVTZ partial optimization at this CN bond length followed by a harmonic frequency calculation provides the model for the vibrations of the transition state in this simple dissociation model.

The combined results from models of the electron detachment and NO_2^- dissociation rates from nitrobenzene anion are shown in the lower panel of Fig. 5. The densities and sums of states were calculated utilizing the Beyer–Swinehart method [85] and at the relevant energies showed close agreement with the results using the Whitten and Rabinovitch approximation [86]. As discussed above, for the detachment rate model an outgoing electron energy of 0.01 eV was assumed, with a correlated capture cross-section of 3.8×10^{-21} m^2 [14]. The scaled harmonic vibrational frequencies for the neutral and anion listed in Table 1 were used to calculate the vibrational sum and density of states. Due to the 1.00 eV adiabatic electron affinity and the outgoing electron energy the sum of states for the neutral is calculated at an energy 1.01 eV lower than the energy of the anion. The energy axis shown in Fig. 5 corresponds to the total amount of energy available in the anion, thus including the 0.01 eV electron energy and the neutral thermal energy (0.10 eV at 300 K), the threshold for electron detachment would be expected a little above 1.1 eV to produce a room-temperature neutral nitrobenzene molecule. The bond dissociation energy of the neutral listed in Table 4 is for 0 K, so this energy is corrected for thermal energies by calculating the difference in the internal thermal energy between $C_6H_5NO_2^-$ and the C_6H_5 and NO_2^- products, which is 0.067 eV at 300 K. Thus, for the dissociation model, the sum of states of the transition state was calculated by removing the imaginary frequency and using an energy of 1.73 eV below that of the anion to correspond to the experimental threshold bond dissociation energy at thermal temperatures.

The detachment model shows a satisfactory agreement with the experimentally observed lifetimes of nitrobenzene metastable anions [11,12]; a reasonable estimate of the detachment threshold in the anion should include some degree of thermal energy in the neutral, and the predicted rate at thermal energies slightly above threshold correlates roughly to millisecond lifetimes. The comparison is somewhat ambiguous as recent studies have suggested that the autodetachment rates of the anions are comprised of a wide distribution of rates [87], and there is a significant spread in the measured values, but the model produces a rate in the correct range at threshold. The model employed here is obviously simplified, for instance, the suggested distribution of ejected electron velocities [82] is not employed, but nonetheless the representative rate curve is of a reasonable magnitude and character. The rate of dissociation is also of reasonable magnitude, and compares favorably to the dissociation rate on the order of 10^9 s^{-1} observed for 3-fluoronitrobenzene anion with an internal energy of 1 eV above threshold [49]. The typical competition between decomposition channels with different activation energies and entropic character is apparent. The combined yields from the calculated rates in a 10 μs detection window is shown in the upper panel of Fig. 5, and comparison to the decomposition channels of the IRMPD spectrum in Fig. 1 shows a good agreement with the model in terms of the ratios of parent depletion to fragment yields. The model suggests a range of the achieved internal energy of the irradiated anions that shows a maximum below 2.5 eV. While the internal energies of the irradiated anions are actually comprised by a wide distribution [75], the competition between the channels constrains the ratio for each characteristic energy, thus providing a 'ceiling' for the detachment yield at high anion internal energy. To test this prediction of the model, a low resolution scan of the nitrobenzene anion dissociation and detachment was acquired at varying FEL laser powers. Previous studies of IRMPD dynamics have established proportionality between laser power and the internal energy of the irradiated ion [49,75]. Shown in Fig. 6 are the depletion, dissociation and detachment yields from these scans, and displayed in the right panel of the figure are the ratios obtained by integrating the dissociation and the detachment yields over the wavelength domain shown. The statistical model correctly predicts the behavior of the competition between the two decomposition channels as the overall importance of the dissociation process increases with laser power.

Evidence for the upper limit of the detachment yield predicted by the statistical model is also observed. Comparison of the spectral peaks at ~1350 and 1260 cm^{-1} is particularly illustrative as the peak at 1350 cm^{-1} is nearing the maximum yield for detachment and the dissociation process is becoming increasingly significant, while the peak at 1260 $cm^{-1}$is not resulting in an ion population with the same degree of internal excitation from the intermediate laser intensities, thus the detachment yield continues to grow towards the maximum yield value.

Although the relationship between the laser power and the distribution of internal energies achieved is complicated, increasing the laser power allows for the input of more internal energy into the anions, shifting the observed ratio towards the higher energy dissociation channel. This agrees with the earlier experimental studies of Han and Brauman [49] who found the higher energy dissociation channel of 3-fluoronitrobenzene to become competitive with the lower energy detachment channel only at high CO_2 laser fluences. Interestingly, it was stated that the fluorinated nitrobenzene was chosen for a detailed analysis of competition between detachment and dissociation because their activation energies are closer to each other than is the case for nitrobenzene. Here, such competition is clearly manifested in the nitrobenzene anion as well, suggesting that higher internal energies are being reached in the present experiment. The ability to access higher energy channels is facilitated by the on-resonance irradiation induced here as compared to the use of fixed-frequency IR sources in the previous study. The success of the statistical model to account for the behavior of the anions under increasingly higher laser power demonstrates that the use of validated spectroscopic parameters can greatly improve the accuracy of these types of models and suggest that implementation of more sophisticated modeling would prove fruitful. The presented model gives a roughly quantitative account of the internal energies of the irradiated ion achieved, thus providing a means to better understand and manipulate the IRMPD process for studies of negative ion dynamics.

4. Conclusions

The infrared vibrational spectrum of the isolated gas-phase nitrobenzene radical anion has been acquired by action spectroscopy methods and analyzed in terms of the vibrations of benzene and nitrobenzene neutral molecules. The IRMPD vibrational frequencies show a very good agreement with those determined by matrix-IR methods. The good agreement of the experimental data with DFT scaled harmonic frequency calculations provides confidence in the calculated bonding characteristics such as molecular orbitals, charge distributions, and barriers to internal rotation, all of which support the postulate of a strong resonance interaction of the NO_2 and phenyl group in the anion. While as a whole the vibrational frequencies are red-shifted relative to the neutral due to the formation of an open-shell anion, there are very instructive individual shifts in frequency and intensity that directly relate to the importance of the CN resonance interaction and the distonic character of the radical anion. The IRMPD action spectrum manifests a competition between the processes of electron detachment and dissociation and this competition is modeled within the framework of statistical unimolecular dissociation theory. The models show a good qualitative agreement with the laser power dependence of the IRMPD process.

Acknowledgments

We acknowledge the excellent support of Drs. Britta Redlich and Lex van der Meer as well as others of the FELIX staff, and thank H. Alvaro Galue and Prof. Robert N. Compton for helpful discussions. This work is part of the research program of FOM, which is financially supported by the Nederlandse Organisatie voor Wetenschappelijk Onderzoek (NWO). Support by the Stichting Physica is gratefully acknowledged.

Appendix A. Supplementary data

Supplementary data associated with this article can be found, in the online version, at doi:10.1016/j.ijms.2011.08.001.

References

[1] K.M. Ervin, J. Ho, W.C. Lineberger, The Journal of Physical Chemistry 92 (1988) 5405–5412.
[2] C. Desfrancois, V. Periquet, S.A. Lyapustina, T.P. Lippa, D.W. Robinson, K.H. Bowen, H. Nonaka, R.N. Compton, The Journal of Physical Chemistry 111 (1999) 4569.
[3] R.F. Gunion, M.K. Gilles, M.L. Polak, W.C. Lineberger, International Journal of Mass Spectrometry and Ion Processes 117 (1992) 601–620.
[4] G.B. Ellison, P.C. Engelking, W.C. Lineberger, Journal of the American Chemical Society 100 (1978) 2556–2558.
[5] R.N. Compton, J.H.S. Carman, C. Desfrancois, H. Abdoul-Carime, J.P. Schermann, J.H. Hendricks, S.A. Lyapustina, K.H. Bowen, The Journal of Chemical Physics 105 (1996) 3472–3478.
[6] C.L. Adams, H. Schneider, K.M. Ervin, J.M. Weber, The Journal of Chemical Physics 130 (2009) 074307.
[7] J.R. Eyler, Mass Spectrometry Reviews 28 (2009) 448–467.
[8] D.H. Geske, A.H. Maki, Journal of the American Chemical Society 82 (1960) 2671–2676.
[9] S. Nagakura, M. Kojima, Y. Maruyama, Journal of Molecular Spectroscopy 13 (1964) 174–192.
[10] R. Ma, D. Yuan, M. Chen, M. Zhou, The Journal of Physical Chemistry A 113 (2009) 1250–1254.
[11] L. Suess, Y. Liu, R. Parthasarathy, F.B. Dunning, The Journal of Physical Chemistry 122 (2005) 124315.
[12] R.N. Compton, L.G. Christophorou, G.S. Hurst, P.W. Reinhardt, The Journal of Physical Chemistry 45 (1966) 4634.
[13] A. Modelli, M. Venuti, International Journal of Mass Spectrometry 205 (2001) 7–16.
[14] A. Pelc, P. Scheier, T.D. Märk, Vacuum 81 (2007) 1180–1183.
[15] P.W. Harland, J.C. Thynne, Journal of the Chemical Society, Chemical Communications 8 (1972) 476.
[16] W.T. Naff, R.N. Compton, C.D. Cooper, The Journal of Chemical Physics 54 (1971) 212–222.
[17] C.L. Adams, H. Schneider, J.M. Weber, The Journal of Physical Chemistry A 114 (2010) 4017–4030.
[18] M.A. Duncan, International Journal of Mass Spectrometry 200 (2000) 545–569.
[19] L.a.P.M. MacAleese, Mass Spectrometry Reviews 26 (2007) 583–605.
[20] M.E. Jacox, Chemical Society Reviews 31 (2002) 108–115.
[21] J. Oomens, J.D. Steill, The Journal of Physical Chemistry A 112 (2008) 3281–3283.
[22] J.D. Steill, J. Oomens, The Journal of Physical Chemistry A 113 (2009) 4941–4946.
[23] J. Oomens, J.D. Steill, B. Redlich, Journal of the American Chemical Society 131 (2009) 4310–4319.
[24] B. Chiavarino, M.E. Crestoni, S. Fornarini, F. Lanucara, J. Lemaire, P. Maitre, D. Scuderi, International Journal of Mass Spectrometry 270 (2008) 111–117.
[25] J. Oomens, J. Steill, Journal of the American Society for Mass Spectrometry 21 (2010) 698–706.
[26] S. Ard, N. Mirsaleh-Kohan, J.D. Steill, J. Oomens, S.B. Nielsen, R.N. Compton, The Journal of Chemical Physics 132 (2010) 094301–094312.
[27] J.D. Steill, J. Oomens, Journal of the American Chemical Society 131 (2009) 13570–13571.
[28] D. Scuderi, C.F. Correia, O.P. Balaj, G. Ohanessian, J. Lemaire, P. Maitre, A European Journal of Chemical Physics and Physical Chemistry 10 (2009) 1630–1641.
[29] J. Oomens, J.D. Steill, T.H. Morton, Inorganic Chemistry 49 (2010) 6781–6783.
[30] G.S. Groenewold, J. Oomens, W.A.d. Jong, G.L. Gresham, M.E. McIlwain, M.J.V. Stipdonk, Physical Chemistry Chemical Physics 10 (2008) 1192–1202.
[31] C.M. Leavitt, J. Oomens, R.P. Dain, J. Steill, G.S. Groenewold, M.J. Van Stipdonk, Journal of the American Society for Mass Spectrometry 20 (2009) 772–782.
[32] R.P. Dain, C.M. Leavitt, J. Oomens, J.D. Steill, G.S. Groenewold, M.J. Van Stipdonk, Rapid Communications in Mass Spectrometry 24 (2010) 232–238.
[33] N.L. Pivonka, C. Kaposta, G. von Helden, G. Meijer, L. Woste, D.M. Neumark, K.R. Asmis, The Journal of Chemical Physics 117 (2002) 6493–6499.
[34] E. Garand, T. Wende, D.J. Goebbert, R. Bergmann, G. Meijer, D.M. Neumark, K.R. Asmis, Journal of the American Chemical Society 132 (2009) 849–856.
[35] K.R. Asmis, G. Santambrogio, M. Brümmer, J. Sauer, Angewandte Chemie International Edition 44 (2005) 3122–3125.
[36] D.T. Moore, J. Oomens, J.R. Eyler, G. Meijer, G. vonHelden, D.P. Ridge, Journal of the American Chemical Society 126 (2004) 14726–14727.
[37] J.D. Steill, J. Oomens, J.R. Eyler, R.N. Compton, The Journal of Chemical Physics 129 (2008) 244302–244308.
[38] P. Kupser, J.D. Steill, J. Oomens, G. Meijer, G. von Helden, Physical Chemistry Chemical Physics 10 (2008) 6862.

[39] D.J. Goebbert, T. Wende, L. Jiang, G. Meijer, A. Sanov, K.R. Asmis, The Journal of Physical Chemistry Letters 1 (2010) 2465–2469.
[40] J.C. Bopp, J.R. Roscioli, M.A. Johnson, T.M. Miller, A.A. Viggiano, S.M. Villano, S.W. Wren, W.C. Lineberger, The Journal of Physical Chemistry A 111 (2007) 1214.
[41] C.L. Lugez, M.E. Jacox, R.A. King, H.F. Schaefer, The Journal of Physical Chemistry 108 (1998) 9639.
[42] J. Fulara, M. Jakobi, J.P. Maier, Chemical Physics Letters 211 (1993) 227–234.
[43] D.M. Wetzel, J.I. Brauman, Chemical Reviews 87 (1987) 607–622.
[44] R.C. Dunbar, International Journal of Mass Spectrometry 200 (2000) 571–589.
[45] G. von Helden, I. Holleman, G.M.H. Knippels, A.F.G. van der Meer, G. Meijer, Physical Review Letters 79 (1997) 5234.
[46] N. Mirsaleh-Kohan, W.D. Robertson, R.N. Compton, Mass Spectrometry Reviews 27 (2008) 237–285.
[47] R.N. Rosenfeld, J.M. Jasinski, J.I. Brauman, The Journal of Physical Chemistry 71 (1979) 1030.
[48] F.K. Meyer, J.M. Jasinski, R.N. Rosenfeld, J.I. Brauman, Journal of the American Chemical Society 104 (1982) 663–667.
[49] C.-C. Han, J.I. Brauman, The Journal of Physical Chemistry 94 (1990) 3403–3415.
[50] J.J. Valle, J.R. Eyler, J. Oomens, D.T. Moore, A.F.G. van der Meer, G. von Helden, G. Meijer, C.L. Hendrickson, A.G. Marshall, G.T. Blakney, Review of Scientific Instruments 76 (2005) 023103.
[51] A.G. Marshall, T.C. Wang, T.L. Ricca, Journal of the American Chemical Society 107 (1985) 7893.
[52] T.H. Mize, I. Taban, M. Duursma, M. Seynen, M. Konijnenburg, A. Vijftigschild, C.V. Doornik, G.V. Rooij, R.M.A. Heeren, International Journal of Mass Spectrometry 235 (2004) 243–253.
[53] D. Oepts, A.F.G. van der Meer, P.W. van Amersfoort, Infrared Physics & Technology 36 (1995) 297–308.
[54] M. Frisch, GAUSSIAN03 Revision C.02, Gaussian Inc., Wallingford, CT, USA, 2004.
[55] A.K. Grafton, R.A. Wheeler, Computer Physics Communications 113 (1998) 78–84.
[56] A.K. Grafton, R.A. Wheeler, Journal of Computational Chemistry 19 (1998) 1663–1674.
[57] E.P. Grimsrud, G. Caldwell, S. Chowdhury, P. Kebarle, Journal of the American Chemical Society 107 (1985) 4627–4634.
[58] J.H.S. Green, D.J. Harrison, Spectrochimica Acta Part A: Molecular Spectroscopy 26 (1970) 1925–1937.
[59] J. Clarkson, W. Ewen Smith, Journal of Molecular Structure 655 (2003) 413–422.
[60] C.V. Stephenson, W.C. Coburn Jr., W.S. Wilcox, Spectrochimica Acta 17 (1961) 933–946.
[61] J.D. Laposa, Spectrochimica Acta Part A: Molecular Spectroscopy 35 (1979) 65–71.
[62] V.A. Shlyapochnikov, L.S. Khaikin, O.E. Grikina, C.W. Bock, L.V. Vilkov, Journal of Molecular Structure 326 (1994) 1–16.
[63] E.B. Wilson, Physical Review 45 (1934) 706.
[64] G. Herzberg, Molecular Spectra and Molecular Structure: Vol. II, Infrared and Raman Spectra of Polyatomic Molecules, Van Nostrand (1945).
[65] L.A. Carreira, T.G. Towns, Journal of Molecular Structure 41 (1977) 1–9.
[66] K.B. Borisenko, I. Hargittai, Journal of Molecular Structure 382 (1996) 171–176.
[67] M. Head-Gordon, J.A. Pople, Chemical Physics Letters 173 (1990) 585–589.
[68] R.A. King, J.M. Galbraith, H.F. Schaefer, The Journal of Physical Chemistry 100 (1996) 6061.
[69] G.L. Gutsev, R.J. Bartlett, Molecular Physics 94 (1998) 121.
[70] C.W. Bauschlicher, A. Ricca, The Journal of Physical Chemistry A 102 (1998) 4722–4727.
[71] M.W. Chase, NIST-JANAF Thermochemical Tables, fourth ed., AIP, Woodbury, NY, USA, 1998.
[72] W.R. Stevens, B. Ruscic, T. Baer, The Journal of Physical Chemistry A 114 (2010) 13134–13145.
[73] S. Xu, M.C. Lin, The Journal of Physical Chemistry B 109 (2005) 8367–8373.
[74] G. Fayet, L. Joubert, P. Rotureau, C. Adamo, The Journal of Physical Chemistry A 112 (2008) 4054–4059.
[75] J. Oomens, B.G. Sartakov, G. Meijer, G. v. Helden, International Journal of Mass Spectrometry 254 (2006) 1–19.
[76] H.M. Rosenstock, M.B. Wallenstein, A.L. Wahrhaftig, H. Eyring, Proceedings of the National Academy of Sciences of the United States of America 38 (1952) 667.
[77] M.L. Vestal, The Journal of Physical Chemistry 41 (1964) 3997.
[78] C.E. Klots, The Journal of Physical Chemistry 46 (1967) 1197.
[79] W.T. Naff, C.D. Cooper, R.N. Compton, The Journal of Physical Chemistry 49 (1968) 2784.
[80] M. Cannon, L. Suess, F.B. Dunning, J.D. Steill, R.N. Compton, The Journal of Physical Chemistry 127 (2007) 064314.
[81] M. Cannon, C.H. Wang, Y. Liu, F.B. Dunning, J.D. Steill, The Journal of Chemical Physics 130 (2009) 244311–244319.
[82] J. Troe, T.M. Miller, A.A. Viggiano, The Journal of Chemical Physics 130 (2009) 244303–244312.
[83] R.A. Marcus, O.K. Rice, Journal of Physical and Colloid Chemistry 55 (1951) 894.
[84] T. Baer, P.M. Mayer, Journal of the American Society for Mass Spectrometry 8 (1997) 103–115.
[85] T. Beyer, D.R. Swinehart, Communications of the ACM 16 (1973) 379.
[86] G.Z. Whitten, B.S. Rabinovitch, The Journal of Physical Chemistry 38 (1963) 2466.
[87] A. Vorob'ev, N. Asfandiarov, V. Lukin, G. Lomakin, Technical Physics 54 (2009) 1255–1262.